Ultra-wideband Aided Precision Parking for Wireless Power Transfer to Electric Vehicles in Real Life Scenarios

Janis Tiemann, Johannes Pillmann, Stefan Böcker and Christian Wietfeld
TU Dortmund University, Communication Networks Institute (CNI)
Otto-Hahn-Str. 6, 44227 Dortmund, Germany
{janis.tiemann, johannes.pillmann, stefan.boecker, christian.wietfeld}@tu-dortmund.de

***Abstract*—Ultra-wideband wireless positioning technologies based on IEEE 802.15.4a have gained attention for various use cases requiring highly precise localization. In this paper an ultra-wideband based approach is proposed and validated for a vehicular use case requiring highly precise local positioning in a dedicated parking lot. For efficient power transfer in wireless charging of electric vehicles scenarios, an accurate alignment of the coils of vehicle and ground is essential. The specific challenge addressed in this paper is that the proposed approach achieves the required lateral accuracy with only two ground-based anchor nodes in combination with one vehicle-based node. For the in-depth validation of the proposed system concept, two experiments are performed: the first one is conducted with an electric vehicle representing a real park-to-charge-case, whereas the second experiment is executed in a controlled environment to allow for further alignment error analysis. The experiments show, that an error lower than 10 cm can be achieved.**

***Keywords*—Ultra-wideband (UWB), Precision Parking, Wireless Power Transfer (WPT), Vehicle to Infrastructure (V2I), Electric Vehicle (EV).**

I. Introduction and Related Work

The resulting shortcoming from the limited capacity of its battery and hence the short reachable range leaves the electric vehicle unable to actually compete with the classical fuel-based counterparts. Wireless power transfer (WPT) is widely considered as a promising solution towards enabling charging without any user interaction. This approach is based on the wireless energy transfer via the primary coil in the charging system, and the secondary coil in the electric vehicle (EV).

The success of this process relies on the achievable transfer efficiency, which is limited by the distance and the alignment between the coils [1].

In order to achieve sufficient coupling efficiency $\eta \geq 90\%$, the coils need to be arranged above each other with a misalignment of roughly five percent of the vehicle's width [2]. Meeting this requirement is barely achieved by manual driving, and the Global Navigation Satellite System (GNSS) receivers can not deliver such performance, this leads to the need for a local high precision alignment system.

In contrast to many other received signal strength based approaches in wireless positioning, ultra-wideband (UWB) systems are capable of accurate time of arrival (TOA) measurements. Due to regulatory decisions and the definition of IEEE 802.15.4a [3], new complementary metal-oxide-semiconductor (CMOS) based UWB systems are seen as the basis of future wireless positioning [4].

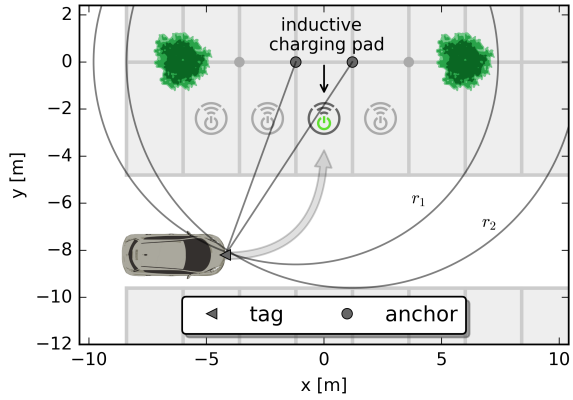

Fig. 1. Illustration of the parking scenario for inductive charging. Note: the set of anchors used for positioning is defined by the chosen parking lot.

Extensive research went into the theoretical limits of a UWB ranging and positioning accuracy, which promises an accuracy in the millimeter range [5]. However, practical systems [6] and [7], relying on recent developments in integrated hardware, are achieving accuracies in the sub 10 cm range. As shown in [8], the high bandwidth provides the ability to resolve multipath propagation, which makes it a viable candidate for parking scenarios especially in the urban environment. The combination of UWB ranging with sensor fusion for indoors automated guided vehicles is presented in [9]. An augmentation system to improve GNSS based results is proposed in [10].

In this paper, a UWB positioning system is untilized as an accurate solution [6], suitable for outdoor as well as indoor scenarios, due to its low energy consumption and the small size of its comprising modules, which makes the upgrade of any park place without notable extra costs easily possible.

Besides the accurate TOA estimation, the used low-cost modules are also easily integrated and used for scenarios requiring high data-rate multi-purpose Vehicle to Infrastructure (V2I) or Vehicle to Vehicle (V2V) communication. Those properties will insure a widespread adoption of the UWB transceivers in the vehicular industry.

A comparable system to the one used in this work is proposed in [11], which covers the issue of autonomous vehicle guidance in GPS-denied environments. This system uses up to 12 anchors and implements a position-velocity based Kalman filter, achieving position accuracies in the sub 30 cm range. However, an experimental evaluation of UWB in the precision parking context, with a minimal set of anchors, to the best of the authors knowledge, has not been conducted.

The park-to-charge test environment is realised as depicted in Fig. 1. Here, the round time of flight (RTOF) is measured and the distance from the tag within the EV to the active ranging anchors is calculated.

An extended Kalman filter (EKF) is used to improve the UWB system's overall accuracy in comparison to raw data positioning. The evaluation of the experiments shows that the alignment error can be kept below 10 cm with a 95 % probability.

Furthermore, to allow for related research and result comparision, the raw ranging readings used for the experiments are published in [12].

II. High Precision Positioning

In the following a detailed desciption of the proposed methodologies applied is given. The communication in form of the high precision clock error eliminating ranging protocol is discussed. Based on the rangings obtained from message exchange, the positioning and mutlipath rejection methods are explained.

A. Ranging Protocol

In order to be independent from any external service or connection, the modules should be capable of dynamically communicating their position and status to any vehicle. Therefore, our approach defines a basic protocol for parking slot registration and ranging, this is depicted in Fig. 2. The tag is initializing the communication with a *txInit* message. If anchors are in range, they will respond with a *txStatus* message, indicating their current Extended Unique Identifier (EUI), position and neighbouring slot information. Once a free slot with two corresponding anchors has been found, the positioning phase is initiated. The tag starts sequential Symmetric Double-Sided Two-Way Ranging (SDS-TWR) [13] with each anchor by sending targeted *txPoll* messages. The polling is answered by the anchors with an a priori known delay t_{dpoll} within *txResp* message. To eliminate the local clock drift, a third *txFinal* message is sent by the tag after t_{dresp}. Since both delays are a priori known, the measured round trip times t_{rpoll} and t_{rresp} are sufficient to calculate the signal propagation time t_p as shown in (1). This enables the i^{th} anchor to calculate the estimated range r_i. In a fourth and last message *txReport*, the anchor reports r_i to the tag.

$$t_p = \frac{t_{rpoll} - t_{dpoll} + t_{rresp} - t_{dresp}}{4} \tag{1}$$

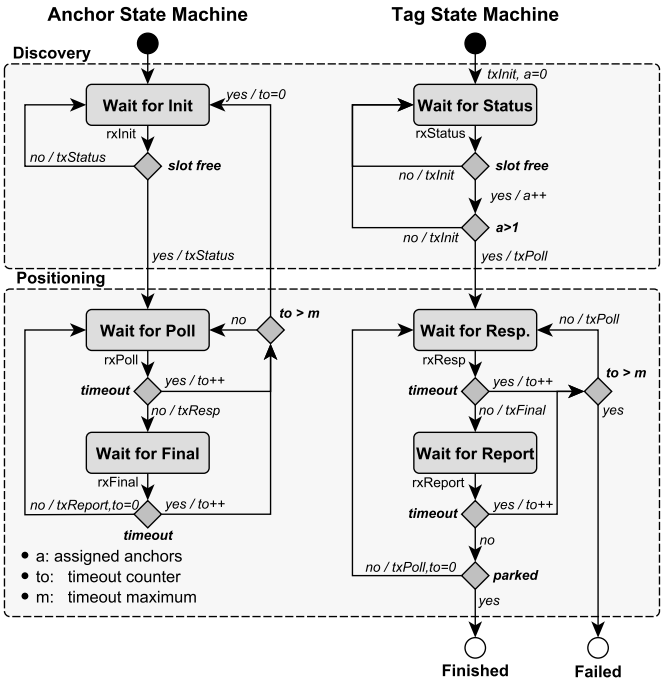

Fig. 2. State machines of the proposed protocol, enabling communication between anchor and tag. The upper part is handling discovery and registration, the lower part implements SDS-TWR.

B. Positioning Methods

The constellation shown in Fig. 1, is the minimal set required for positioning in two-dimensional plane. Several aspects of the proposed scenario are exploited to ensure positioning with two anchors. It is assumed, that both the height of the anchors h_i and the height of the tag h_t are known. Hence, the range in the two-dimensional plane is calculated by

$$r_i = \sqrt{d_i^2 + (h_t - h_i)^2} \tag{2}$$

Where d_i is the measured range in the three-dimensional plane. For self-localization, the tag is sequentially ranging with the anchors, obtaining the measured ranges r_i to each anchor i. Since each range is measured with an error e_i, the true geometrical distance ρ_i is unknown. The euclidean distance ρ_i of the position of the i^{th} anchor (x_i, y_i) to the tag's position (x_t, y_t) is defined by (3).

$$r_i = \rho_i + e_i = \sqrt{(x_i - x_t)^2 + (x_i - y_t)^2} + e_i \tag{3}$$

Usually, an overdefined set of equations is used for positioning. In the special case of this work, the position may be calculated in a closed form algorithm. A circle intersection is sufficient to obtain two possible solutions for the vehicle position. To improve the results an EKF similar to [14] is implemented to exploit the Gaussian distribution of the ranging measurements. In this specific constellation the Jacobian of the measurements $\boldsymbol{H}_k$ is calculated by equation (4)

$$\boldsymbol{H}_k = \begin{bmatrix} -\frac{x_1 - x_{t,k}}{\hat{\rho}_{1,k}} & -\frac{y_1 - y_{t,k}}{\hat{\rho}_{1,k}} \\ -\frac{x_2 - x_{t,k}}{\hat{\rho}_{2,k}} & -\frac{y_2 - y_{t,k}}{\hat{\rho}_{2,k}} \end{bmatrix} \tag{4}$$

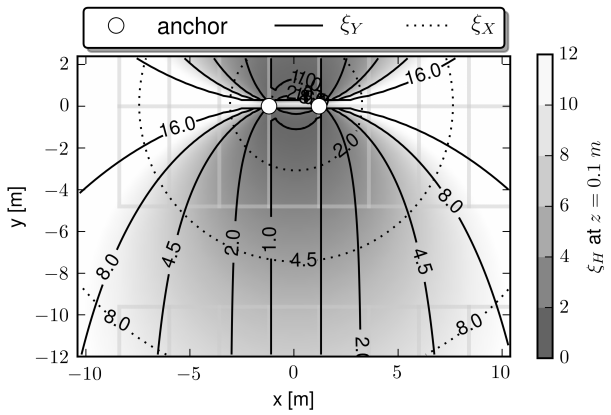

Fig. 3. Positioning error gain ξ_H dependent on the position of the vehicle. A lower ξ_H yields for better positioning capabilities. Note the difference between vertical and horizontal error gain ξ_X and ξ_Y.

Where $\hat{\rho}_{i,k}$ is the euclidean distance of the estimated position at step k to the anchor i.

Although vehicles are often modeled with Constant Turn Rate and Velocity (CTRV) [15], or even more complex state models, this work utilises a more generalized approach, namely a Position-Velocity (PV) one, due to inavailability of the turn rate and the velocity sensors. The PV model is suitable for the position based filtering, its state vector is defined as $\boldsymbol{x}_k = [x \quad y \quad \dot{x} \quad \dot{y}]^\top$.

C. Constellation Quality

One of the most important aspects in wireless positioning is the geometry of the anchor distribution. In Time-Difference-of-Arrvial (TDOA) based satellite systems, the ability to position at a certain point in this constellation is described by the Dilution of Precision (DOP) [16]. This concept is an indicator for the error gain depending on the satellite constellation. Since the ranging with UWB systems is TOA based, this concept is adopted slightly modified in this work. The covariance matrix $\boldsymbol{Q}_k$ is calculated as given in equation (5) with the help of the aforementioned Jacobian of measurements $\boldsymbol{H}_k$.

$$\boldsymbol{Q}_k = \left(\boldsymbol{H}_k^\top \boldsymbol{H}_k\right)^{-1} \tag{5}$$

The diagonal elements of $\boldsymbol{Q}_k$ are the variances σ_x^2 and σ_y^2. The value of interest for this scenario is the horizontal error gain ξ_H which is calculated by equation (6).

$$\boldsymbol{\xi}_X = \sqrt{\sigma_x^2} \qquad \boldsymbol{\xi}_Y = \sqrt{\sigma_y^2} \qquad \boldsymbol{\xi}_H = \sqrt{\sigma_x^2 + \sigma_y^2} \tag{6}$$

In Fig. 3, the scenario constellation listed in Tab. I is evaluated in terms of positioning capability. Depending on the vehicle's position, the error gain along the x-axis is given by $\boldsymbol{\xi}_X$. The error gain along the y-axis by $\boldsymbol{\xi}_Y$ and the combined horizontal error gain by $\boldsymbol{\xi}_H$.

TABLE I. ANCHOR POSITIONS

EUI	x [m]	y [m]	z [m]
DECA020000000002	1.20	0.00	0.38
DECA020000000003	-1.20	0.03	0.38

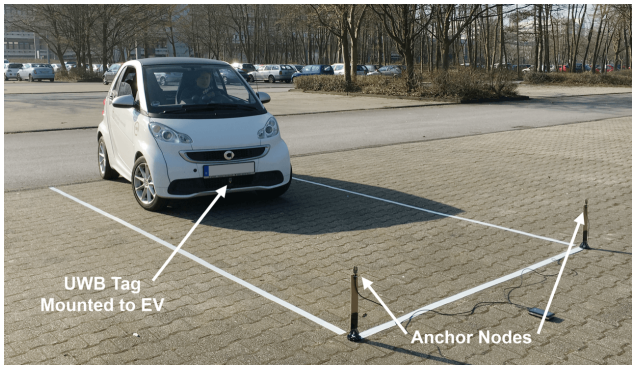

Fig. 4. Experimental setup in the realistic environment. The lower front of the EV was equipped with an UWB tag. A typical parking procedure was performed. Note the small footprint of the parking slot installation.

D. Multipath Rejection

Due to the high temporal resolution of UWB, the channel impulse response (CIR) of the received signals may be evaluated at the receiver. The correlation of the received signal with the reference pulse [3] allows not only for accurate TOA estimation by detection of the first path, but may also be used to gain information of the channel itself. The used transceiver allows access to a register holding those correlation results. The power of the first detected path P_{fp} is compared to the accumulated power over the CIR P_{cir}.

$$\phi_{fp}[dB] = P_{fp}[dBm] - P_{cir}[dBm] \tag{7}$$

Since reflected signals hold less power and more ambiguity than signals received from the direct path, a metric ϕ_{fp}, indicating potential non-line-of-sight (NLOS) conditions is introduced in equation (7) to differentiate and reject measurements with potentially erroneous values. The resulting metric may be used in two ways. A simple threshold based rejection is the safest way to ensure NLOS signals are ignored. This

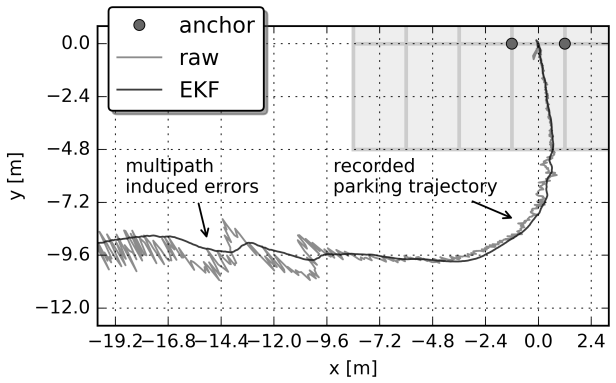

Fig. 5. Experimental results of the realistic parking procedure. Note the change in the variation of the raw, unfiltered positioning results as the EV is approaching the parking slot.

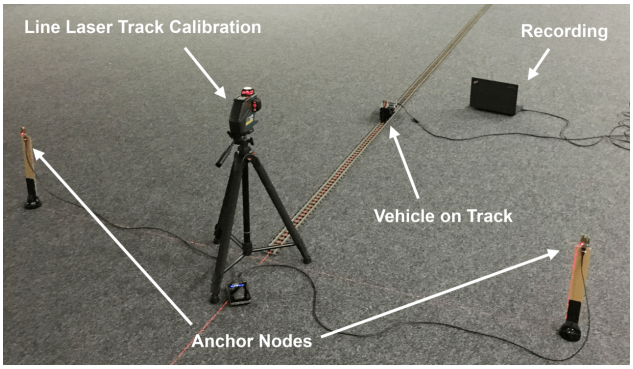

Fig. 6. Experimental setup illustrating the controlled environment. A track with a length of 8.5m was precisely aligned with a self-nivelling 3D line laser.

comes with the cost of loosing rangings needed for positioning, leading to a decreasing temporal resolution. Next to rejection of samples, a weighting scheme similar to [17] may be used to weight the ranges with the propability of being NLOS. This allows for graceful system degradation.

III. Experimental Evaluation

To evaluate the performance of the UWB positioning system, two different experiments are conducted. In the first experiment a typical real parking procedure is executed to qualitatively analyze the system performance.

A parking slot is equipped with the UWB anchor nodes. Since the anchors only communicate with the tag, as described in II-A, no extra communication link is needed. This leads to the small system footprint visible in Fig. 4.

The resulting positions of the parking maneuver are depicted in Fig. 5.

It is clearly visible, that the unfiltered parking trajectory is strongly dependend on the distance to the parking slot, this is due to the constellation dependend parameter $\boldsymbol{\xi}_H$ explained in II-C. However, the results close to the parking slot and

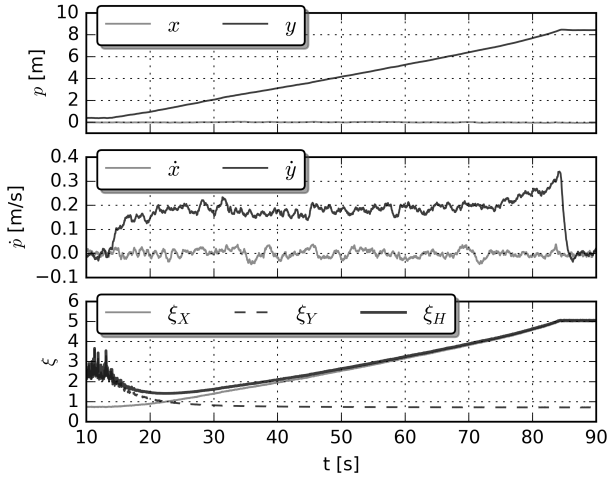

Fig. 7. Time series of the controlled environment experiment. Depicted is the EKF state in position $p = [x, y]$ and velocity $\dot{p} = [\dot{x}, \dot{y}]$. Note the development of the error gain $\boldsymbol{\xi}_X$, $\boldsymbol{\xi}_Y$ and $\boldsymbol{\xi}_H$.

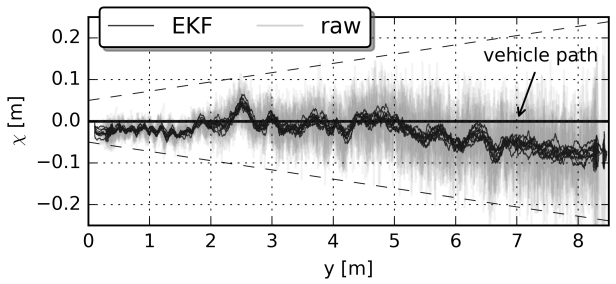

Fig. 8. Experimental results of the track based parking experiment. Depicted are the EKF positionial state and the raw positioning results. Note the different scaling of the χ and y axis.

especially on the parking slot itself show little variation which indicate small errors. Since the vehicle is not movable in a reference movement and due to the lack of an outdoor reference system, a second experiment is conducted to quantitavely assess the alignment accuracy.

In order to analyze and quantify the alignment error in the parking process, the vehicle needs to be moved on a defined track, shown in Fig. 6 illustrating the set up of the second experiment resembling parking in a straight way.

A motorized vehicle runs in a controlled manner along a line-laser calibrated track. For statistical confidence, this process was repeated several times. To provide reproducable results, the raw data is published [12]. A time series of this experiment is shown in Fig. 7. The EKF state vector $\boldsymbol{x}_k = [x \;\; y \;\; \dot{x} \;\; \dot{y}]^\top$ is shown over the experiment execution time. The positionial components x and y as well as the estimated speeds $\dot{x}$ and $\dot{y}$ are depicted. Due to the controlled movement the position on the track y increases linearily. Therefore, the speed along the track $\dot{y}$ is nearly constant at 0.2m/s between t = 20 s and t = 80 s. Due to the change in position, the error gain $\boldsymbol{\xi}_X$ increases over time, when $\boldsymbol{\xi}_Y$ decreases. Since $\boldsymbol{\xi}_H$ is the upper bound of $\boldsymbol{\xi}_X$ and $\boldsymbol{\xi}_Y$ it has a minimum at t = 23 s where $\boldsymbol{\xi}_X$ and $\boldsymbol{\xi}_Y$ intersect.

The results are shown in Fig. 8. Since the true position on the x-axis is known, the alignment error χ is given through the x-coordinate. It is visible that the raw positioning accuracy calulated as proposed in II follows an envelope given through $\boldsymbol{\xi}_X$. Also, the results of all the repetitions follow a similar trajectory. This correlation indicates systematic errors to be accounted for by a calibration or other compensation methods. The range around y = 1 m shows the least variation in the alignment error. Obviously, this is directly linked to the minimum in the error gain $\boldsymbol{\xi}_X$ discussed in II-C.

The cumulative distribution $\Phi(\chi)$ of the absolute alignment error χ in the alignment phase is illustrated in Fig. 9. It should be noted, that for comparable error analysis the beginning

TABLE II. Error quantiles for the alignment error χ.

	$Q(50\%)$ [m]	$Q(75\%)$ [m]	$Q(90\%)$ [m]	$Q(95\%)$ [m]	$Q(99\%)$ [m]
EKF	0.024	0.046	0.070	0.081	0.095
raw	0.031	0.057	0.097	0.127	0.184
improv.	29%	23%	38%	57%	93%

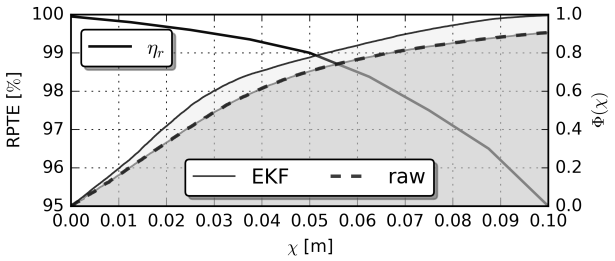

Fig. 9. Cumulative distribution $\Phi(\chi)$ of the absolute alignment error χ in nine experiments. Note the improvement of the EKF over the raw positioning. The exemplary [1] relative power transmission efficiency (RPTE) of η_r is giving an indicator for the efficiency achievable dependent on χ.

and the end of the experiment is removed, similar to the presentation in Fig. 7. Quantiles are used to quantify the probability of an error below a certain value, see Tab. II. Evidently the EKF is improving the results compared to the raw position calculation in all cases. Since the scenario requires a high reliability, the $Q(95\%)$ quantiles are analyzed. With a probability of 95 %, the error is under 15 cm for the position calculated via raw positioning. For the EKF filtered position, the error is significantly reduced to under 10 cm. To assess this accuracy in the context of wireless power transfer, the relative power transmission efficiency (RPTE) of a pratical system η_r [1], is evaluated over the achieved alignment error. For EKF based positioning the relative power transmission efficiency is $\eta_r > 95\%$, whereas for raw positioning $\eta_r > 90\%$. The accuracy of the proposed UWB positioning system is therefore enabling high efficiency wireless power transfer, necessary for high power automotive applications.

IV. Conclusion and Future Work

This paper introduces a UWB based positioning system for precision parking. This system utilizes highly integrated 802.15.4a RF hardware and a minimal set of anchors. Futhrmore, an upgrade of the existing parking slots requires no massive changes, due to the low-cost small sized modules comprising the proposed system. A metric for the positioning capabilities was introduced for the specific TWR based setup. Two independent experiments were conducted for qualitative and quantitative evaluation. An alignment accuracy of under 10 cm is achieved on the parking slot in 95 % of the cases. The overall system capabilities were shown to be more than sufficient for precision coil alignment of automotive grade wireless power transfer, allowing for relative transfer efficiencies of $\eta_r > 90\%$.
Future work will use NLOS metric based weighting, diverse sensors and therefore a more elaborate vehicle model, allowing for better position filtering and robustness.

The raw experimental datasets are provided alongside this work.

Acknowledgement

The work on this paper has been partially funded by Deutsche Forschungsgemeinschaft (DFG) within the Collaborative Research Center SFB 876 “Providing Information by Resource-Constrained Analysis”, project A4/B4 and has received funding in the course of the SyncFuel project from the German Federal Ministry of Transport and Digital Infrastructure (BMVi) under grant number 03EM0614A.

References

[1] Wei Ni, I.B. Collings, Xin Wang, Ren Ping Liu, A. Kajan, M. Hedley, and M. Abolhasan. Radio alignment for inductive charging of electric vehicles. *Industrial Informatics, IEEE Transactions on*, 11(2):427–440, Apr 2015.

[2] S. Hasanzadeh, S. Vaez-Zadeh, and A.H. Isfahani. Optimization of a contactless power transfer system for electric vehicles. *Vehicular Technology, IEEE Transactions on*, 61(8):3566–3573, Oct 2012.

[3] IEEE Std 802.15.4-2011: Part 15.4: Low-Rate Wireless Personal Area Networks (LR-WPANs). http://standards.ieee.org/getieee802/download/802.15.4-2011.pdf.

[4] M.R. Mahfouz, A.E. Fathy, M.J. Kuhn, and Y. Wang. Recent trends and advances in UWB positioning. In *Wireless Sensing, Local Positioning, and RFID, 2009. IMWS 2009. IEEE MTT-S International Microwave Workshop on*, pages 1–4, Sep 2009.

[5] C. Zhang, M. Kuhn, B. Merkl, M. Mahfouz, and A.E. Fathy. Development of an UWB indoor 3D positioning radar with millimeter accuracy. In *Microwave Symposium Digest, 2006. IEEE MTT-S International*, pages 106–109, Jun 2006.

[6] J. Tiemann, F. Schweikowski, and C. Wietfeld. Design of an UWB indoor-positioning system for UAV navigation in GNSS-denied environments. In *Indoor Positioning and Indoor Navigation (IPIN), 2015 International Conference on*, Oct 2015.

[7] V. Kristem, S. Niranjayan, S. Sangodoyin, and A.F. Molisch. Experimental determination of uwb ranging errors in an outdoor environment. In *Communications (ICC), 2014 IEEE International Conference on*, pages 4838–4843, Jun 2014.

[8] J.M. Cramer, R.A. Scholtz, and M.Z. Win. Spatio-temporal diversity in ultra-wideband radio. In *Wireless Communications and Networking Conference, 1999. WCNC. 1999 IEEE*, pages 888–892 vol.2, 1999.

[9] R. G. Yudanto and F. Petre. Sensor fusion for indoor navigation and tracking of automated guided vehicles. In *Indoor Positioning and Indoor Navigation (IPIN), 2015 International Conference on*, pages 1–8, Oct 2015.

[10] K. O'Keefe, Yuhang Jiang, and M. Petovello. An investigation of tightly-coupled UWB/low-cost GPS for vehicle-to-infrastructure relative positioning. In *Radar Conference, 2014 IEEE*, pages 1295–1300, May 2014.

[11] F. Hartmann, F. Pistorius, A. Lauber, K. Hildenbrand, J. Becker, and W. Stork. Design of an embedded uwb hardware platform for navigation in gps denied environments. In *Communications and Vehicular Technology in the Benelux (SCVT), 2015 IEEE Symposium on*, pages 1–6, Nov 2015.

[12] J. Tiemann. Raw dataset, http://dx.doi.org/10.5281/zenodo.47343. Mar 2016.

[13] R. Hach and A. Rommel. Wireless synchronization in time difference of arrival based real time locating systems. In *Positioning Navigation and Communication (WPNC), 2012 9th Workshop on*, pages 193–195, Mar 2012.

[14] R. Khan, F. Sottile, and M.A. Spirito. Hybrid positioning through extended kalman filter with inertial data fusion. *International Journal of Information and Electronics Engineering*, 2013.

[15] R. Schubert, C. Adam, M. Obst, N. Mattern, V. Leonhardt, and G. Wanielik. Empirical evaluation of vehicular models for ego motion estimation. In *Intelligent Vehicles Symposium (IV), 2011 IEEE*, pages 534–539, Jun 2011.

[16] R. B. Langley. Dilution of precision. *GPS world*, May 1999.

[17] T. Dammes and R. Kays. Soft-decision based position estimation for wireless localization in indoor scenarios. In *Positioning Navigation and Communication (WPNC), 2013 10th Workshop on*, pages 1–6, Mar 2013.